Supplementary Materials

Crystal facet engineering induced robust and sinter-resistant Au/α-MnO_2 catalyst for propane efficient oxidation: Indispensable role of oxygen vacancy and $Au^{\delta+}$ species

Yanfei Jian[a], Zeyu Jiang[a], Chi He[a,b,*], Mingjiao Tian[a], Weiyu Song[c], Guanqun Gao[a], Shouning Chai[a,*]

[1]*State Key Laboratory of Multiphase Flow in Power Engineering, School of Energy and Power Engineering, Xi'an Jiaotong University, Xi'an 710049, Shaanxi, P.R. China*

[2]*National Engineering Laboratory for VOCs Pollution Control Material & Technology, University of Chinese Academy of Sciences, Beijing 101408, P.R. China*

[3]*State Key Laboratory of Heavy Oil Processing, China University of Petroleum, Beijing 102249, P.R. China*

[*]To whom correspondence should be addressed:

Tel./Fax: +86 29 82663857

E-mail: chi_he@xjtu.edu.cn (C. He)

Tel./Fax: +86 29 82668572

E-mail: chaishn2019@xjtu.edu.cn (S.N. Chai)

Text S1. Experimental section

Text S1.1. Catalyst preparation

(1) Synthesis of α-MnO_2-310. α-MnO_2-310 was synthesized *via* a hydrothermal redox reaction between $KMnO_4$ and $(NH_4)_2C_2O_4$. In a typical procedure, 20 mmol of $KMnO_4$ and 10 mmol of $(NH_4)_2C_2O_4 \cdot H_2O$ were dissolved into 70 mL of deionized water under vigorous magnetic stirring. The mixture solution was then transferred to a 100 mL Teflon-lined stainless-steel autoclave and heated at 180 °C for 24 h. After the autoclave cooled naturally to room temperature, the precipitates were collected by centrifugation, washed several times with deionized water, and then dried at 105 °C to form a black powder. Finally, the as-obtained powder was calcined in air at 300 °C for 4 h (heating rate of 5 °C min-1) to obtain the α-MnO_2-310 sample.[1]

(2) Synthesis of α-MnO_2-110. α-MnO_2-110 was prepared by the same synthesis route as for α-MnO_2-310, but the reductance of $(NH_4)_2C_2O_4$ was replaced by $(NH_4)_2SO_4$.[1]

(3) Synthesis of α-MnO_2-100. α-MnO_2-100 was prepared by a hydrothermal redox reaction of $MnSO_4 \cdot H_2O$, $(NH_4)_2S_2O_8$, and $(NH_4)_2SO_4$.[2] In a typical procedure, 8 mmol of $MnSO_4 \cdot H_2O$, 8 mmol of $(NH_4)_2S_2O_8$, 15 mmol of $(NH4)_2SO_4$, and 8 mmol of KNO_3 were dissolved in 40 mL of deionized water under vigorous magnetic stirring. Then, the above solution was transferred into a 100 mL Teflon-lined stainless-steel autoclave and kept at 120°C for 20 h. After the autoclave cooled naturally to room temperature, the precipitates were collected by centrifugation, washed several times with deionized water, and dried at 105 °C to form a black powder. Finally, the as-obtained powder was calcined in air at 300 °C for 4 h (heating rate of 5 °C min-1) to obtain the α-MnO_2-100 sample.[1]

(4) Synthesis of Au/MnO_2 catalysts. The *in situ* reduction method[3] was used to prepare

Au/MnO_2 catalysts with chloroauric acid and ascorbic acid as precursor and reducing agent, respectively. The theoretical Au loading was 2 wt%. Typically, 0.204 g of PVP was dissolved into 300 mL of deionized water under stirring at 80 ℃, and then 36 mg of $HAuCl_4 \cdot 3H_2O$ (with 18 mg Au equivalent) was added dropwise. Meanwhile, 0.9 g of MnO_2 powder was dispersed in 150 mL of deionized water by ultrasonic treatment in advance and added to the above solution and continuously stirred. After 6 h, 30 mL of 0.1 $mol \cdot L^{-1}$ ascorbic acid was added to the solution and stirred for another 1 h. Afterwards, the precipitate was recovered by suction filtration, washed repeatedly with deionized water and absolute ethanol, and dried at 60 ℃ for 16 h. Finally, the powder was calcinated in a muffle furnace at 300 ℃ for 4 h with a heating rate 1 ℃ min^{-1} to obtain the Au/MnO_2 catalysts.

Text S1.2. Catalyst characterizations

N_2-sorption isotherms were measured at 77 K on a Micromeritics ASAP 2020 apparatus. Prior to the measurements, the samples were evacuated for 14 h under vacuum at 473 K. X-ray diffraction (XRD) measurements were performed using a Rigaku powder diffractrometer (Rigaku, Japan) with Cu-Ka radiation. The tube voltage was 45 kV, and the current was 40 mA. All diffraction patterns were obtained in 2θ range of 10-80° with a scan speed of 2° min^{-1}. The micromorphology and chemical composition of prepared materials were examined by a field-emission scanning electron microscope (FE-SEM; JSM-6500F) operated at 15 kV and a high-resolution transmission electron microscope (HR-TEM; JEM-3000F) operated at 300 kV with a point-to-point resolution of 0.17 nm equipped with an electron energy loss spectrometer. The magnetic properties were characterized by vibrating sample magnetometry. The electron field-emission behavior was measured in a vacuum of 1×10^{-7} Torr using a spherical stainless steel

probe (1 mm in diameter) as the anode. The lowest emission current was recorded on the level of nanoamps. The measurement distance between the anode and the emitting surface was fixed at 100 μm. X-ray photoelectron spectroscopy (XPS) was carried out on a RBD upgraded PHI-5000C ESCA system (Perkin-Elmer) with Mg-Kα radiation ($h\nu$ = 1253.6 eV). The X-ray anode was run at 250 W, and the high voltage was maintained at 14.0 kV with a detection angle at 54°. The pass energy was fixed at 93.90 eV to ensure sufficient resolution and sensitivity. The base pressure of the analyzer chamber was approximately 5×10^{-8} Pa. The entire spectra (0-1100 eV) and narrow spectra of all elements were both recorded with extremely high resolution by using a RBD 147 interface (RBD Enterprises, USA) through the XPS Peak4.1 software. Binding energies were calibrated using the carbon (C 1*s* = 284.6 eV). Hydrogen temperature-programmed reduction (H_2-TPR) experiments were performed on a PCA-1200 (Builder, China) analyzer. 50 mg of catalysts were heated from RT to 800 °C at 10 °C min^{-1} under a mixture of 5 *vol.*%H_2/Ar (15 mL min^{-1}). Hydrogen consumption was measured using a thermal conductivity detector (TCD). For C_3H_8-TPSR, the sample (50 mg) was pretreated with N_2 at 300 °C for 30 min, and then cooled to room temperature. The sample in 5% C_3H_8/N2 flow (40 mL/min) was heated at a rate of 10 K/min. A mass spectrometer (HPR20 QIC) was used to monitor the effluent gas and the MS signal of C_3H_6 (m/z = 41), C_3H_8 (m/z = 29), CO_2 (m/z = 12) and CO_2 (m/z = 44) was recorded. Fourier transform infrared (FTIR) absorption spectra were recorded at room temperature on a Tensor 37 (Bruker, Germany) FTIR spectrometer with 32 scans at an effective resolution of 4 cm^{-1}. Raman spectra in the range of 100~1500 cm^{-1} were obtained on a RM2000 laser Raman spectrometer by employing excitation wavelength of 532 nm line of Ar ion laser and recorded on a LabRam spectrometer (JobinYvon Horiba). The wavelength was calibrated using Si signal at 520 cm^{-1}.

In situ diffuse reflectance infrared Fourier transform spectroscopy (*in situ* DRIFTS) of propane oxidation was performed on a Bruker Vertex 70 (Bruker, Germany) infrared spectrometer equipped with a mercury cadmium telluride (MCT) detector cooled by liquid nitrogen. Reaction cell (Harrick Scientific, USA) was fitted with KBr windows and connected to a purging and adsorption gas control system. The total flow rate was controlled by mass flow meter (D07-19B, Sevenstar Electronics, China). Prior to the catalytic oxidation experiments, catalyst samples were pre-treated under N_2 at 400 °C for 1 h to remove the surface impurities. The spectrum of catalyst powder was taken at every selected reaction temperatures in a N_2 flow, which was subtracted from the corresponding spectrum of the catalyst and the reaction mixture in the cell. The activated catalyst was contacted with a flow of a gas mixture, containing 2500 ppm propane/20% O_2/N_2 in temperature range of 25-230 °C. The system reached a new steady state in about 20-25 min, as verified by the stabilized MS peak intensity. All spectra were collected at a resolution of 4 cm^{-1} with 100 scans.

Text S1.3. Catalytic activity

All evaluation experiments were performed in a continuous flow fixed-bed reactor, consisting of a steel tube (6 mm, i.d.) at atmospheric pressure. In each test, 1.0 mL of catalyst (40-60 mesh) was placed in the tube reactor. The pollutant containing gas was generated by bubbling air through the VOC saturator, which was further diluted with another air stream before reaching the reaction bed (C_3H_8 concentration of 2500 ppm). The total flow rate was kept at 200 mL min^{-1}, *i.e.*, a gas hourly space velocity (GHSV) of 12,000 h^{-1}. The reaction bed temperature increased to the following setting and maintained for 30 min for online detection before the next experimental procedure. The concentration of C_3H_8 was measured by a GC-9890B online gas chromatography

(Linghua, China) equipped with a flame ionization detector (FID) and a HT-Wax column. The quantitative analyses of CO_2 and CO were carried on GC with Ni-FID.

The conversion of C_3H_8 ($X_{C_3H_8}$) was calculated by Eq. (1),

$$X_{C_3H_8} = \frac{[C_3H_8]_{in} - [C_3H_8]_{out}}{[C_3H_8]_{in}} \quad (1)$$

where $[C_3H_8]_{in}$ and $[C_3H_8]_{out}$ represent the C_3H_8 concentrations in the inlet and outlet gas, respectively.

The reaction rate ($r_{C_3H_8}$, mmol mL^{-1} h^{-1}) was calculated as Eq. (2),

$$r_{C_3H_8} = \frac{10^3 \cdot 3600 \cdot X_{C_3H_8} \cdot V_{C_3H_8}}{V_{cat}} \quad (2)$$

where V_{cat} represents the catalyst volume (mL), $V_{C_3H_8}$ is the C_3H_8 gas flow rate (mol s^{-1}).

When the conversion of C_3H_8 is < 20 %, a dependence of the reaction rate on the products of CO_2 and H_2O may be ignored, and the empirical kinetic expression of the reaction rate equation of MEK oxidation can be described as Eq. (3),

$$r_{C_3H_8} = A \exp\left(-\frac{E_a}{RT}\right) P_{C_3H_8}^{\alpha} P_{O_2}^{\beta} \quad (3)$$

Taking the natural logarithm of Eq (3), Eq. (4) can be obtained.

$$\ln r = \ln A + \alpha \ln P_{C_3H_8} + \beta \ln P_{O_2} - \frac{E_a}{RT} \quad (4)$$

The components of the reactant feed gas showed minor changes during the kinetics data testing, and the conversion of C_3H_8 was < 20%. Therefore, $\ln A$, $\alpha \ln P_{C_2H_6}$, and $\beta \ln P_{O_2}$ can be supposed to be approximately constant, and Eq. (4) can be simplified to Eq. (5),

$$\ln r = -\frac{E_a}{RT} + C \quad (5)$$

The activation energy (E_a, kJ mol^{-1}) can be obtained from the slope of the resulting linear plot of $\ln r$ versus $1/T$.

Text S1.4. DFT studies

The (110), (310), and (100) surface slabs of α-MnO_2 were considered for study by the first-principles density functional theory (DFT) calculations as implemented in the Vienna Ab initio Simulation Package (VASP)[4] with plane wave basis sets and projector-augmented wave (PAW)[5] pseudopotentials. The electronic structure was calculated using the Generalized Gradient Approximation (GGA) of Perdew-Burke-Ernzerhof with Hubbard U corrections (PBE+U).[6] Previous work demonstrated a good description of lithium intercalation, band gaps, and magnetic interactions when PBE+U was applied in the fully localized limit, which we employ as (U−J) = 4 eV in this work as well. To obtain the equilibrium lattice parameters by relaxation of the bulk cell, a cutoff for the plane wave basis set of 400 eV was used to avoid Pulay stress. According to the results of XRD, the α-MnO_2 crystal occurs in the tetragonal space group I4/m with lattice parameters a = 9.784 Å, b = 9.784 Å, and c = 2.863 Å. All subsequent calculations were performed based upon the obtained equilibrium lattice constants using a cutoff of 400 eV. A vacuum thickness greater than 12 Å was applied to avoid the interaction between the slab and its periodical images. All the ions were iteratively relaxed by a conjugate gradient algorithm until the absolute value of force on each ion converged below to 0.05 eV/Å. Formation energy (E_{vo}) of the oxygen vacancy is defined as follows:

$$E_{vo} = E_{def} - E_{bulk} + \frac{1}{2}E_{O_2} \quad (6)$$

where E_{def} is the system energy with a loss of one oxygen atom (O), E_{bulk} is the energy of a slab without the loss of an oxygen atom, and E_{O_2} is the energy of an O_2 molecule in the gas phase.

Table S1 Comparison of some typical catalysts reported in the literature for propane oxidation.

Sample	Reaction conditions	GHSV[a] ($mL \cdot g_{cat}^{-1} \cdot h^{-1}$)	T_{50}[b] (ºC)	T_{90}[b] (ºC)	*Ref.*
Au/MnO_2-100	2500 ppm C_3H_8 + Air	12,000	189	216	This work
$Ru/ZnAl_2O_4$	0.2 vol.% C_3H_8 + Air	21,000	198	220	7
Pt/ZSM-5	2000 ppm C_3H_8 + 2% O_2/Ar	30,000	220	240	8
Pt/TiO_2	0.8% C_3H_8/9.9% O_2 in N_2	18,000	330	427	9
Pd/SiO_2-Al_2O_3	0.25% C_3H_8/9% O_2 in N_2	1,200,000	507	/	10
1%Au/Co_3O_4	8000 ppm C_3H_8 + Air	12,000	200	220	11

[a] Gas hourly space velocity; [b] Temperatures at which 50% and 90% conversion of propane.

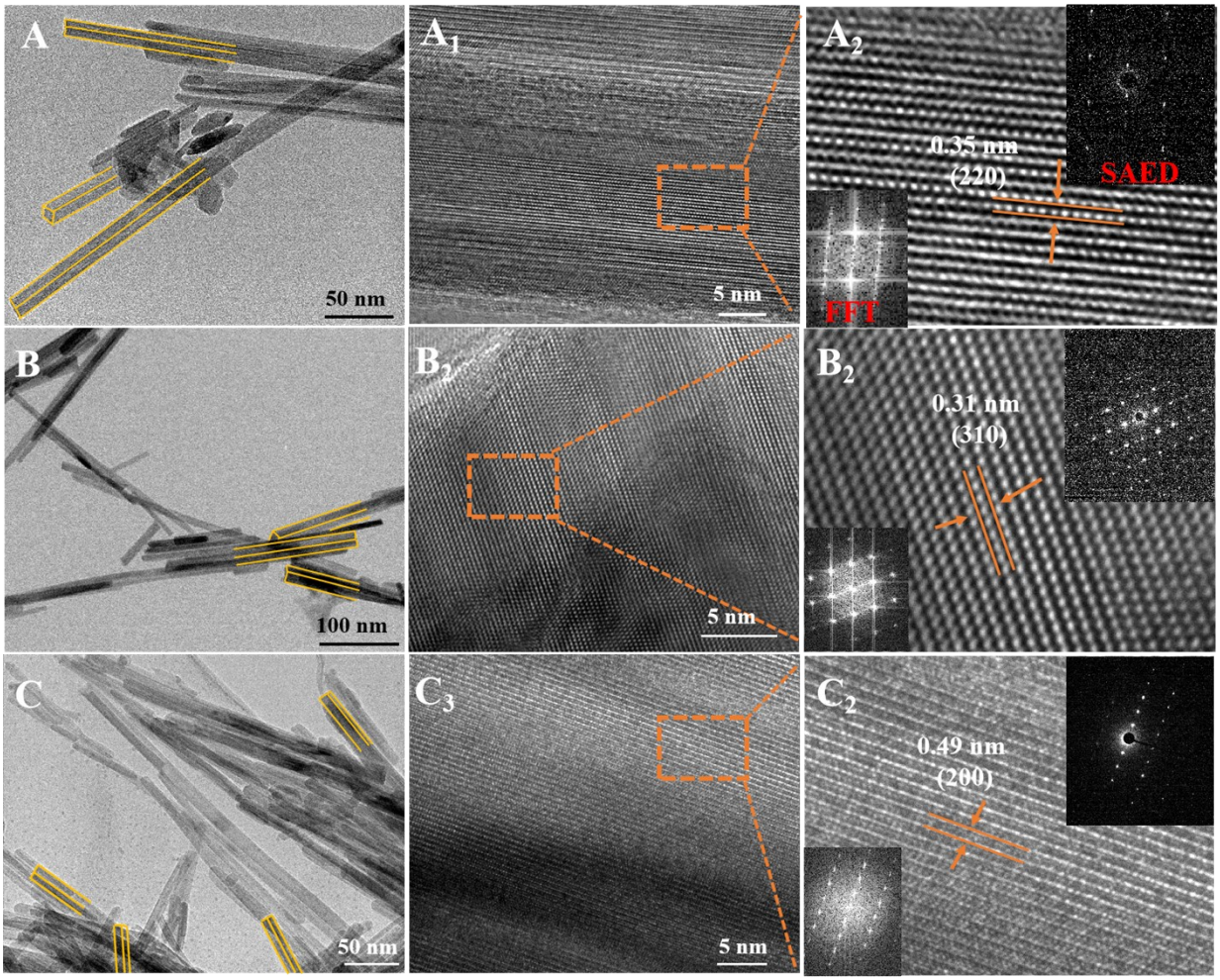

Figure S1 TEM and high-resolution TEM images of MnO_2-110 (A, A_1 and A_2), MnO_2-310 (B, B_1 and B_2) and MnO_2-100 (C, C_1 and C_2) (Insets show the corresponding SAED patterns and FFT patterns)

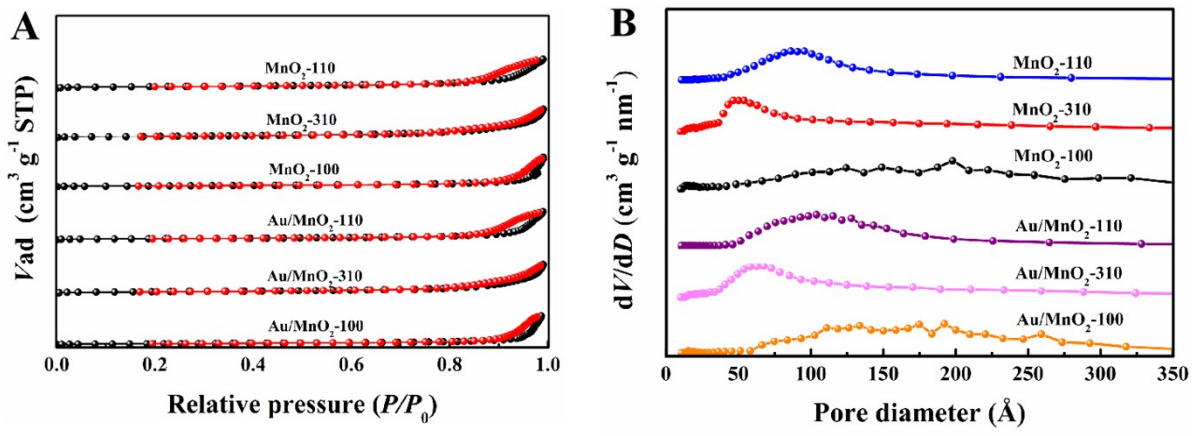

Figure S2 (A) N_2 adsorption/desorption isotherms and (B) corresponding pore size distribution of prepared catalysts.

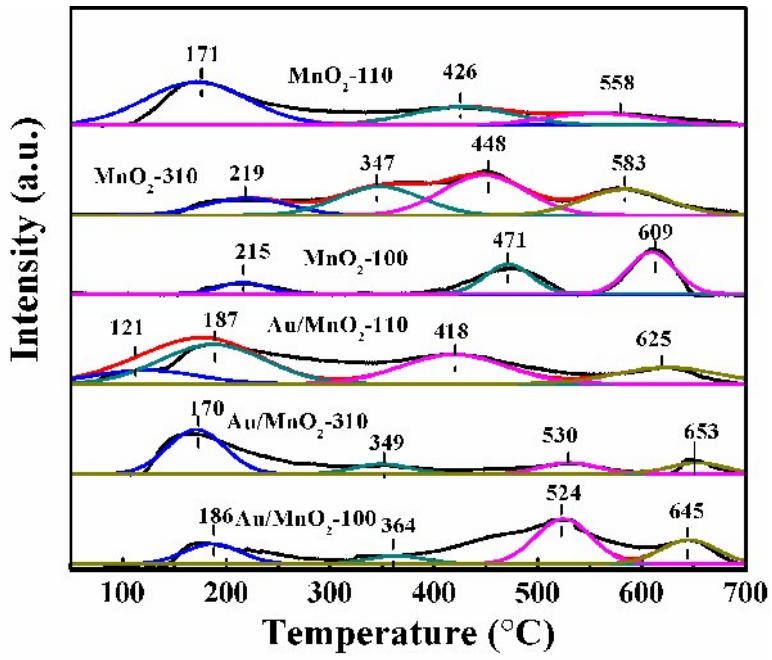

Figure S3 O_2-TPD of different catalysts

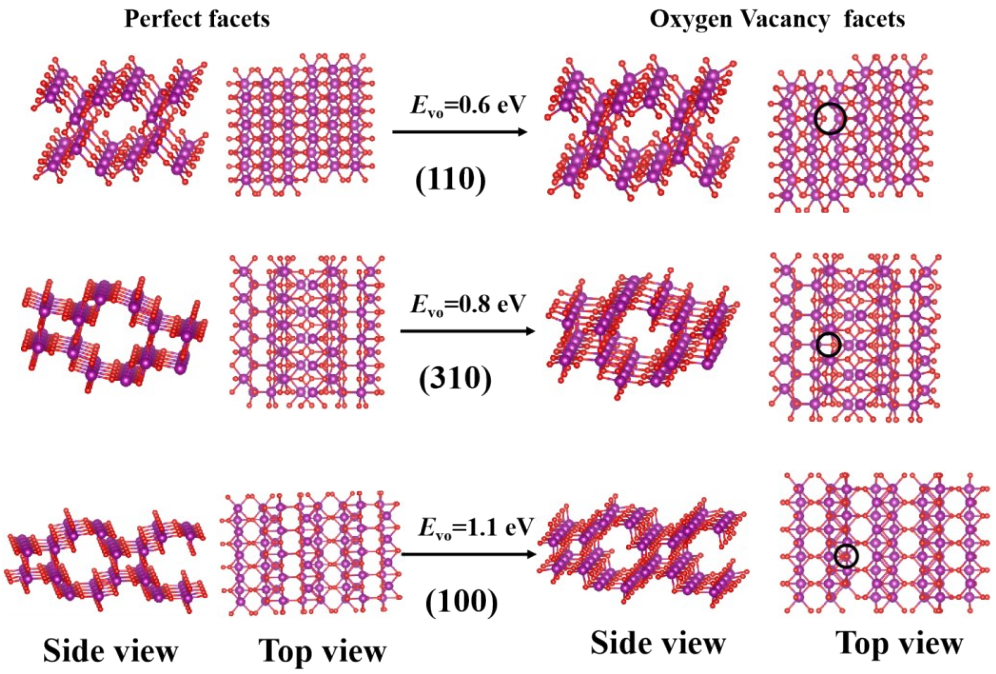

Figure S4 Formation energy of oxygen vacancy over α-MnO_2 with different exposed facets.

Oxygen vacancy is suggested to play an important role in the decomposition of propane,[12] and the activity of a oxide catalyst is largely depends on the property and concentration of oxygen vacancy. In present work, the formation energy of a single O defect at α-MnO_2 exposed facets was studied by DFT calculations. Results demonstrate that the formation energy of oxygen vacancy on (110) facet of α-MnO_2 (E_{vo} (110) = 0.6 eV) is lower than that of (310) (E_{vo} (310) = 0.8 eV) and (100) (E_{vo} (100) = 1.1 eV) facets, indicating that the oxygen vacancies are easier to form on (110) facets MnO_2.

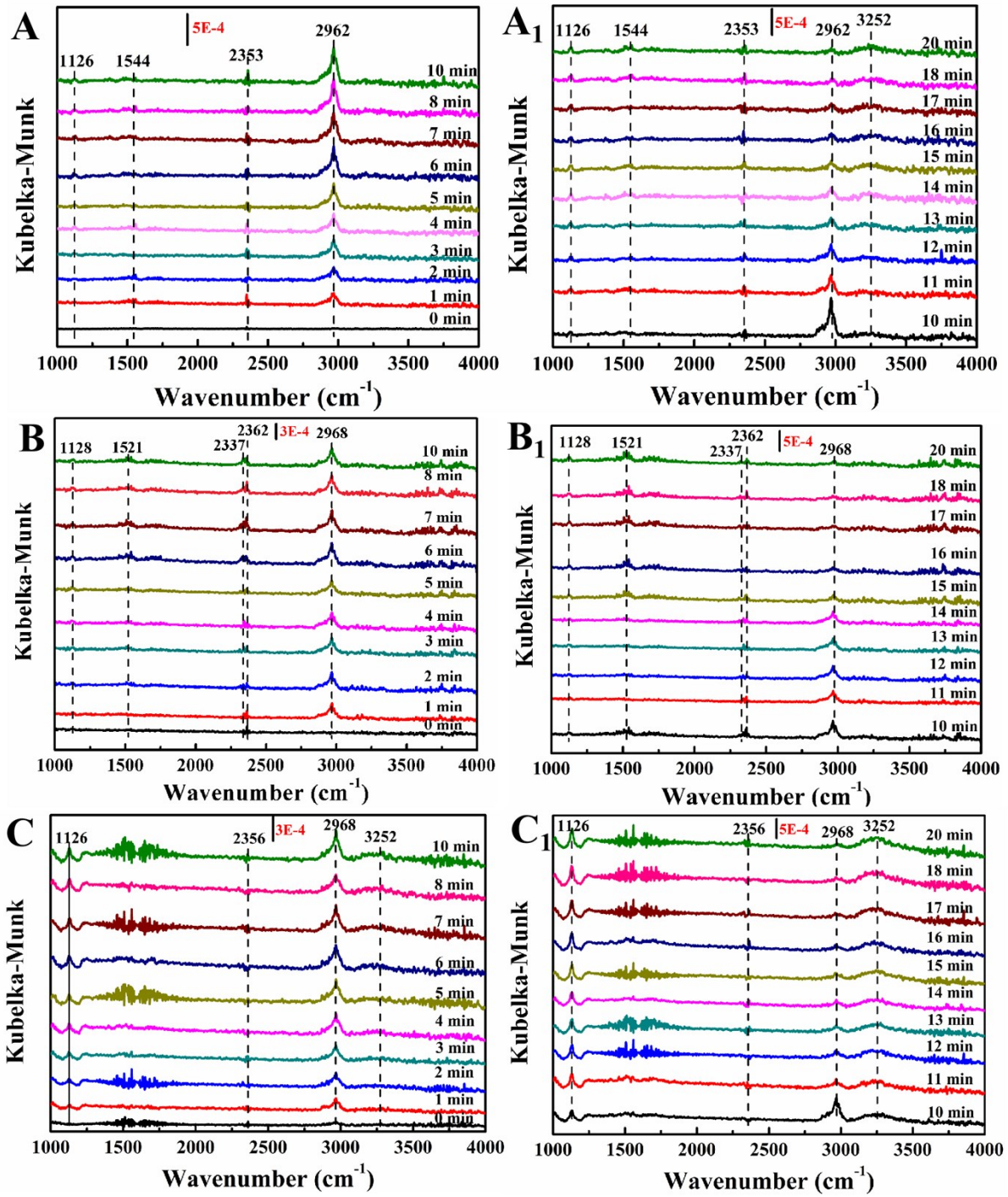

Figure S5 *In situ* DRIFT spectra of (A) Au/MnO_2-110, (B) Au/MnO_2-310, and (C) Au/MnO_2-100 at 230 ℃ in the feed gas (40 mL/min) of 0.25%C_3H_8 + 25%O_2/N_2, and then 25%O_2/N_2 (A_1, B_1, C_1), relative to time (min).

References

1. S. Rong, P. Zhang, F. Liu and Y. Yang, *ACS Catal.,* 2018, 8, 3435-3446.

2. J. T. Hou, L. L. Liu, Y. Z. Li, M. Y. Mao, H. Q. Lv and X. J. Zhao, *Environ. Sci. Technol.,* 2013, 47, 13730-13736.

3. F. Jiang, X. Zhu, B. Fu, J. Huang and G. Xiao, Chin. J. Catal., 2013, 34, 1683-1689.

4. G. Kresse and J. Furthmuller, *Phys. Rev. B,* 1996, 54, 11169-11186.

5. G. Kresse and D. Joubert, *Phys. Rev. B,* 1999, 59, 1758-1775.

6. J. P. Perdew, K. Burke and M. D. Ernzerhof, *Phys. Rev. Lett.,* 1996, 77, 3865-3868.

7. J. Okal and M. Zawadzki, *Appl. Catal. B-Environ.,* 2011, 105, 182-190.

8. Z. Zhu, G. Lu, Y. Guo, Y. Guo, Z. Zhang, Y. Wang and X. Q. Gong, *ChemCatChem,* 2013, 5, 2495-2503.

9. M. S. Avila, C. I. Vignatti, C. R. Apesteguía and T. F. Garetto, *Chem. Eng. J.,* 2014, 241, 52-59.

10. Y. Yazawa, H. Yoshida, N. Takagi, S. Komai, A. Satsum and T. Hattori, *J. Catal.,* 1999, 187, 15-23.

11. B. Solsona, E. Aylon, R. Murillo, A. M. Mastral, Monzonis, A. Agouram, S. T. E. S.Davies, H. Taylor and T. Garcia, *J. Hazard. Mater.,* 2011, 187, 544-52.

12. Y. Jian, T. Yu, Z. Jiang, Y. Yu, Douthwaite, M. Liu, J. Albilali, and C. He, *ACS Appl. Mater. Interfaces,* 2019, 11, 11369-11383.